

# Radiosensitization by microRNA30a-5p in a nude mouse model with subcutaneous lung-cancer xenograft\*

Yuyan Guo<sup>1</sup>, Yingtao Cui<sup>1</sup>, Xing Bao<sup>1</sup>, Yue Ke<sup>1</sup>, Hongtao Ren<sup>1</sup>, Jiyuan Pan<sup>1</sup>, Liping Song<sup>2</sup>, Hongbing Ma<sup>1</sup> (✉)

<sup>1</sup> Department of Radiation Oncology, the Second Affiliated Hospital of Xi'an Jiaotong University, Xi'an 710004, China

<sup>2</sup> Department of Radiation Oncology, the First Affiliated Hospital of Xi'an Jiaotong University, Xi'an 710061, China

## Abstract

**Objective** We aimed to observe the radiosensitization effect of mir-30a-5p in a nude mouse model with subcutaneous lung-cancer xenograft and to explore the underlying mechanism.

**Methods** A549 cell lines with either stable upregulation or downregulation of mir-30a-5p, and their negative control, were transfected with lentivirus vectors. These cell lines were used to establish a nude mouse model with subcutaneous lung-cancer xenograft. Each group was randomly divided into irradiated and non-irradiated groups. The radiosensitization effect of mir-30a-5p *in vivo* was studied by observing xenograft growth trends and tumor weight. The mechanisms involved in this radiosensitization were investigated by detecting expressed radiosensitization-related proteins, using immunohistochemistry and Western blotting.

**Results** The expression level of mir-30a-5p in the lenti-mir-30a-5p group was higher than that in the negative control (lenti-GFP) group and lower in the lenti-inhibitor group ( $P < 0.05$ ). Subcutaneous lung-cancer xenografts in the irradiation group and lenti-mir-30a-5p increased in size slowly; tumors were lighter and tumor inhibition rates were higher than those in the non-irradiation and lenti-GFP groups. In contrast, the opposite of these effects was observed in the lenti-inhibitor group. Immunohistochemistry and Western blotting indicated that ATM protein expression level was lower in the lenti-mir-30a-5p group, with or without irradiation, compared to that in the lenti-GFP group. ATM protein levels were higher in the lenti-inhibitor groups. The phosphorylation level of ATM at residue 1981 was low in the groups without irradiation and increased significantly after irradiation ( $P < 0.05$ ). Moreover, the phosphorylation level was lower in the lenti-mir-30a-5p group and higher in the lenti-inhibitor group than that in the lenti-GFP group after irradiation ( $P < 0.05$ ).

**Conclusion** Mir-30a-5p enhanced the radiosensitivity of nude mice with subcutaneous lung-cancer xenografts by inhibiting ATM phosphorylation.

**Key words:** Mir-30a-5p; subcutaneous xenografts; radiosensitization; ATM

Received: 15 November 2021

Revised: 2 April 2022

Accepted: 21 May 2022

Lung cancer is one of the most common malignant tumors worldwide, of which approximately 80% are non-small cell lung cancer (NSCLC) [1]. Radiotherapy is one of the primary treatments for NSCLC however, radioresistance is common during the treatment of NSCLC. This leads to a local recurrence rate up to 60%–70% and

makes it difficult to achieve the expected curative effect [2]. Therefore, reducing the radioresistance of NSCLC, thereby increasing its radiosensitivity, is the key issue [3]. Various factors could be involved in regulating the radiosensitivity of cancer, such as DNA damage and repair (DDR) [4], cell cycle arrest [5], apoptosis [6], cancer stem cells

✉ Correspondence to: Hongbing Ma. Email: mhbxi@126.com

\* Supported by the National Science Fund Project (No. 81872471) of the National Natural Science Foundation of China and the Science Foundation of the Second Affiliated Hospital of Xi'an Jiaotong University (No. YJ(QN)202025).

© 2022 Huazhong University of Science and Technology

[7], autophagy [8], immunity [9–10]. Additionally, classical cell signaling pathways may be involved, including ataxia telangiectasia mutated (ATM) signal pathway [11], PI3K/AKT (phosphoinositide 3-kinase/AKT serine/threonine kinase), mitogen-activated protein kinase/extracellular regulated protein kinases (MAPK/ERK), and transforming growth factor-beta (TGF- $\beta$ ) signaling pathways [12–13].

Notably, microRNAs play roles in radiosensitization and can affect the radiosensitivity of cancer by modulating a variety of molecules that are involved. These molecules include DNA-dependent protein kinase catalytic subunit (DNA-PKcs), ATM [14], H2AX variant histone (H2A.X), mediator of DNA damage checkpoint 1 (MDC1), epidermal growth factor receptor (EGFR), AKT, and breast cancer susceptibility gene 1 (BRCA1) [11].

Further, mir-30a is downregulated in both NSCLC tissues and cell lines, and that it could influence cell proliferation [15], migration, invasion [16], apoptosis [17], phosphorylation, and participates in mitogen-activated protein kinase (MAPK), TGF- $\beta$ , PI3K/AKT, and other pathways [11, 13]. In a previous study by our group, we found that mir-30a-5p can enhance the radiosensitivity of lung cancer cells A549 by down-regulating activating transcription factor 1 (ATF1) *in vitro* [18]. We conducted this study to further explore if mir-30a-5p can also function as a radiosensitizer *in vivo*.

## Materials and methods

### Animal culture

A total of 36 SPF-grade 3–5-week-old male nude mice, weighing approximately 13–20 g, were housed at a temperature of 22–24 °C and a relative humidity of 50%–70%. All the nude mice were provided by the Animal Experimental Center of the Medical Department of Xi'an Jiaotong University, China.

### Cell lines and main reagents

Human lung adenocarcinoma cell line A549 and human renal epithelial cell line 293T were donated by the Transformation Center Laboratory of the First

Affiliated Hospital of the Medical Department of Xi'an Jiaotong University, China. The main reagents were as follows: mir-30a-5p u vector pGMLV-MA2 and mir-30a-5p downregulation vector pGMLV-MI7 (GenePharma, Shanghai, China), QIAprep Spin Miniprep Kit (QIAGEN, Shanghai, China), T4 DNA ligase (Fermentas, USA), T4 DNA ligase buffer (Fermentas, USA), BamHI (Fermentas, USA), XhoI (Fermentas, USA), Express miRNA Extraction Kit (HaiGene CN, China), PrimeScript™ RT Master Mix (TaKaRa, Japan), Mir-X™ miRNA First-Strand Synthesis Kit (TaKaRa, Japan), SYBR Premix Ex Taq™ II (TaKaRa, Japan), SP immunohistochemical kit (Beijing Zhongshan Jinqiao Biotechnology Co. Ltd., China), and rabbit anti-goat SP kit (BOSTER Biological Technology Co. Ltd., China).

### Cell culture

The human lung adenocarcinoma cell lines A549, A549 with mir-30a-5p overexpression, A549 (with mir-30a-5p downregulation) and a control cell line were cultured in RPMI-1640 medium and 293T cell line in DMEM containing 10% fetal bovine serum. The cells were incubated at 37 °C and 5% CO<sub>2</sub>.

### Lentiviral infection

Primers were synthesized to amplify the pri-miRNA sequence has-mir-30a 5'-primer: 5'-GTG TAA ACA TCC TCG ACT GGA AG-3' (Sangon Biotech, Shanghai, China), and genomic DNA was used as a template. Single-stranded DNA oligomers were synthesized with interference sequences to inhibit the processing of mir-30a-5p (Table 1) and miRNA-inhibitor primer sequences (Table 2) were synthesized by Sangon Biotech (Shanghai, China). The enzyme-digested DNA was directly connected to the lentiviral vector through the end of the endonuclease site BamHI and XhoI. The lentiviral vector and packaging plasmid were co-transfected into 293T cells for lentiviral packaging. The original virus solution was diluted with culture medium containing 5  $\mu$ g/mL polybrene, according to the appropriate MOI value. A549 cells were infected for 48 h, fluorescence was observed, and the infection

**Table 1** pri-miR primer sequence

Name	Sequence
6235-F (XhoI)	5'-CCGCTCGAGCGGTAGTCTAAGTTCACTCAACTGCA-3'
6235-R (BamHI)	5'-CCGGATCCCTGGGAAATATTGCCCTACTACG-3'

**Table 2** miRNA-inhibitor primer sequence

Name	Sequence
hsa-mir-30a-inhibitor-T (BamHI)	5'-gatccGACGGCGCTAGGATCATCAACCTTCCAGTCGAGATCTGATGTTACACAAGTATTCTGGTCACAGAATACAACCTTCCAGTCGAGATCTGATGTTACACAAGATGATCCTAGCGCCGCTTTTTTg-3'
hsa-mir-30a-inhibitor-B (EcoRI)	5'-aattcAAAAAAGACGGCGCTAGGATCATCTTGTGTAACATCAGATCTCGACTGGAAGTTGTATTCTGTGACCAGAATACTTGTGTAACATCAGATCTCGACTGGAAGTTGATGATCCTAGCGCCGTCg-3'

efficiency of A549 cells was estimated.

### qRT-PCR

The total RNA from cells in each group was extracted using the Express miRNA Extraction Kit (HaiGene China), according to the manufacturer's instructions. Using mRNA as a template, random primers or oligo (dT) were used to reverse transcribe cDNA. Hsa-mir-30a-5p gene sequence was queried in NCBI (GenBank No. MI0000088) and used to design primers for qRT-PCR, using Primer version 5.0 (PREMIER Biosoft International, Palo Alto, CA, USA), and synthesized by Sangon Biotech (Shanghai, China): has-mir-30a 5'-primer: 5'-GTG TAA ACA TCC TCG ACT GGA AG-3'. The expression of mir-30a-5p was detected using qRT-PCR.

### Establishment of subcutaneous xenograft model

The lenti-mir-30a, lenti-inhibitor, or lenti-GFP vectors were used to infect A549 cell lines in logarithmic phase, at a final concentration of  $5 \times 10^7$  cells/mL. The cells were mixed with Matrigel at a 1:1 ratio on ice. Nude mice were randomly divided into three groups, with 12 mice in each group, and injected with lenti-mir-30a A549 cells, lenti-inhibitor A549 cells, or lenti-GFP A549 cells. This was conducted subcutaneously, on the back of each nude mouse, with 0.2 mL cell suspensions. Tumorigenesis was observed every other day, and vital signs, body weight, and tumor size of nude mice were recorded.

### Irradiation

When the tumor size was approximately 1.0 cm<sup>3</sup>, the nude mice in each treatment group were randomly divided into radiation and non-radiation groups. Nude mice in the radiation group were given a total of 10 Gy 4 MV X-ray radiation at 200 cGy/d for 5 consecutive days. After irradiation, the tumor volume was measured ( $V = a^2 \times b / 2$ ), the growth and metastasis of the tumor were observed, the nude mice were weighed every day, vital observed, and the tumor growth curves drawn. After observation, the nude mice were sacrificed, tumor tissues removed, and the tumor volume measured. Tumor tissues were fixed in 4% polyformaldehyde solution, then embedded in paraffin, and sections cut.

### Immunohistochemistry

First, hematoxylin and eosin (H&E) staining was performed. Immunohistochemical staining of the paraffin sections was performed using the streptavidin-peroxidase binding method. Put the paraffin sections into a 60 °C constant temperature drying oven for 60 minutes. Then placing the sections in xylene to dewaxing. Dehydrating the paraffin sections through decreasing concentrations

of ethanol, and washing in PBS. Immunostaining was undertaken using the antibodies against ATM (1:200) (Abcam) and ATM (phospho S1981) (4 µg/mL)(Abcam). The sections were placed in a humid chamber and incubated with goat serum for 15 min at 37 °C. The primary antibody was applied to the tissue sections and incubated overnight at 4 °C before incubating with the secondary antibody at 37 °C for approximately 30 min. DAB chromogenic solution (WanleiBio, China) was used to develop the color, according to the manufacturer's instructions. The sections were counter-stained via re-dyeing with hematoxylin, soaked in 1% ammonia water, dehydrated with gradient alcohol, cleared with xylene, and sealed with neutral gum seal. Microscope observation showed that ATM protein was located in the nucleus or cytoplasm. Three fields on each section were randomly selected under 400 × magnification, and the expression intensity was semi-quantitatively analyzed using IPP 6.0 image analysis software (Media Cybernetics, Georgia Avenue, USA). The expression intensity, was expressed as the average optical density value, was defined as the integrated optical density (IOD)/cumulative area.

### Western blotting

Small pieces of tumor tissue were placed in protein extraction reagent (RIPA and protease inhibitors at 50:1). The tissue was homogenized at low speed until it was fully homogenized. The supernatant protein was extracted and quantified, according to the instructions of BCA protein quantitative kit. Proteins were separated according to size, by sodium dodecyl sulfate polyacrylamide gel electrophoresis. The protein was then immobilized on PVDF membrane by electroblotting before blocking to prevent non-specific protein binding. The target proteins were probed by incubating with specific primary antibodies for 12 to 16 h at 4 °C followed by incubation with a secondary antibody for 1 h at 37 °C. The antigen/antibody binding signal was then detected, using a Bio-Rad imaging system, to analyze the densitometry of the protein bands.

### Ethical statement

Animal experiments were performed in accordance with the ethical guidelines for experimental animals of the Department of Medicine, Xi'an Jiaotong University, China.

### Statistical analysis

All data were analyzed using SPSS 21.0 (IBM, USA), and the results are expressed as mean ± SEM. The enumeration data were analyzed by  $\chi^2$  test or Fisher's exact test, and the measurement data were tested using the group *t*-test. Statistical significance was set at  $P < 0.05$ .

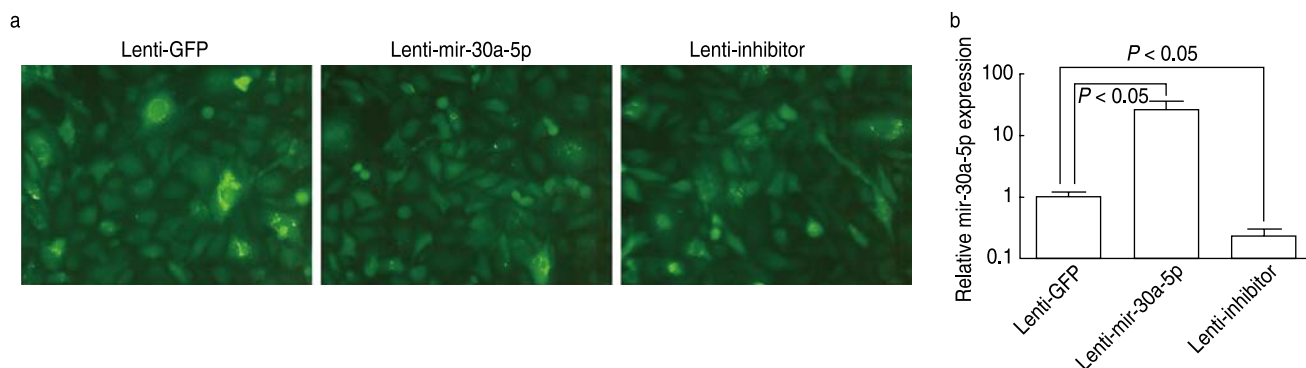


**Fig. 1** Expression of mir-30a-5p in the lentivirus stable transfected A549 cell lines. (a) Green fluorescence expression ( $\times 400$ ); (b) qRT-PCR results for expression of mir-30a-5p

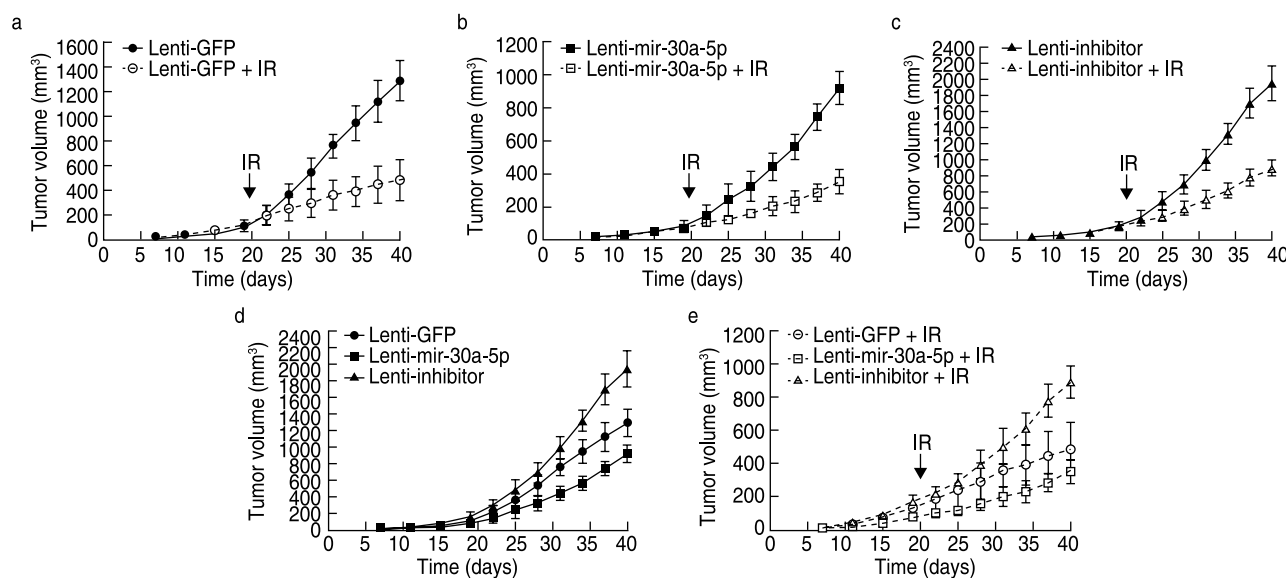


**Fig. 2** Subcutaneous xenograft growth curve in different groups. (a) Lenti-GFP vs. Lenti-GFP + IR; (b) Lenti-mir-30a-5p vs. Lenti-mir-30a-5p + IR; (c) Lenti-inhibitor vs. Lenti-inhibitor + IR; (d) The three groups without irradiation; (e) The three groups with irradiation. IR: irradiation

## Results

### Lentivirus stable infected A549 cell lines were successfully constructed

The presence of green fluorescence was assessed under a fluorescence microscope (Fig. 1a). The qRT-PCR results showed that the expression level of mir-30a-5p in the lenti-mir-30a-5p group was higher than that in the lenti-GFP group ( $P < 0.05$ ). The expression level of mir-30a-5p in the lenti-inhibitor group was lower than that in the lenti-GFP group ( $P < 0.05$ ). This demonstrated that the lentivirus stably infected A549 cell lines with mir-30a-5p overexpression and downregulation were successfully constructed (Fig. 1b).

### Radiosensitization effect of mir-30a-5p in nude mice with subcutaneous lung-cancer xenograft

The tumor volume in the different treatment groups was measured, and the tumor growth curves were drawn (Fig. 2). The results showed that when irradiation began, the volume growth trend of subcutaneous xenografts became slower, and all growth curves became smoother than those in the non-irradiated groups (Fig. 2a–2c). The volume growth trend of subcutaneous xenografts was slower, and the growth curve was smoother in the lenti-mir-30a-5p group than in the lenti-GFP group, with or without irradiation (Fig. 2d–2e). In contrast, in the lenti-inhibitor group, tumors grew faster, and the growth curve was steeper than that in the lenti-GFP group (Fig. 2d–2e).

The tumor weights in the irradiated groups were lower than those in the non-irradiated groups ( $P < 0.05$ ). Tumor weights in the lenti-mir-30a-5p and irradiated lenti-mir-

**Table 3** Tumor weight, body weight of nude mice and tumor inhibition rate in different treatment groups

	Groups	n	Tumor weight (g)	Body weight of nude mice (g)	Tumor inhibition rate <sup>a</sup> (%)	Tumor inhibition rate <sup>b</sup> (%)
Non-IR	Lenti-GFP	3	1.29 ± 0.28	21.83 ± 1.72	–	–
	Lenti-mir-30a-5p	3	0.92 ± 0.18	21.23 ± 1.33	27.86 ± 7.02	27.86 ± 7.02
	Lenti-inhibitor	3	1.94 ± 0.37	20.80 ± 1.30	–	–
IR	Lenti-GFP	3	0.49 ± 0.28*	16.67 ± 0.71**	–	64.47 ± 14.17
	Lenti-mir-30a-5p	3	0.35 ± 0.13*	17.10 ± 0.98*	18.75 ± 22.17	73.16 ± 3.98
	Lenti-inhibitor	3	0.89 ± 0.17*	17.17 ± 1.82*	–	30.53 ± 5.20 <sup>#</sup>

Note: Tumor inhibition rate (%) = (tumor weight in the negative control group – tumor weight in the treatment group) / tumor weight in the negative control group × 100%; <sup>a</sup>: Lenti-GFP group vs. Lenti-mir-30a-5p group or Lenti-GFP + IR group vs. Lenti-mir-30a-5p + IR group; <sup>b</sup>: Lenti-GFP group vs. Lenti-GFP + IR group or Lenti-GFP vs. Lenti-mir-30a-5p + IR group or Lenti-GFP group vs. Lenti-inhibitor + IR group; \*: Non-IR group vs. IR group, *P* < 0.05; \*\*: Non-IR group vs. IR group, *P* < 0.01; <sup>#</sup>: Lenti-GFP + IR group vs. lenti-inhibitor + IR group, *P* < 0.05

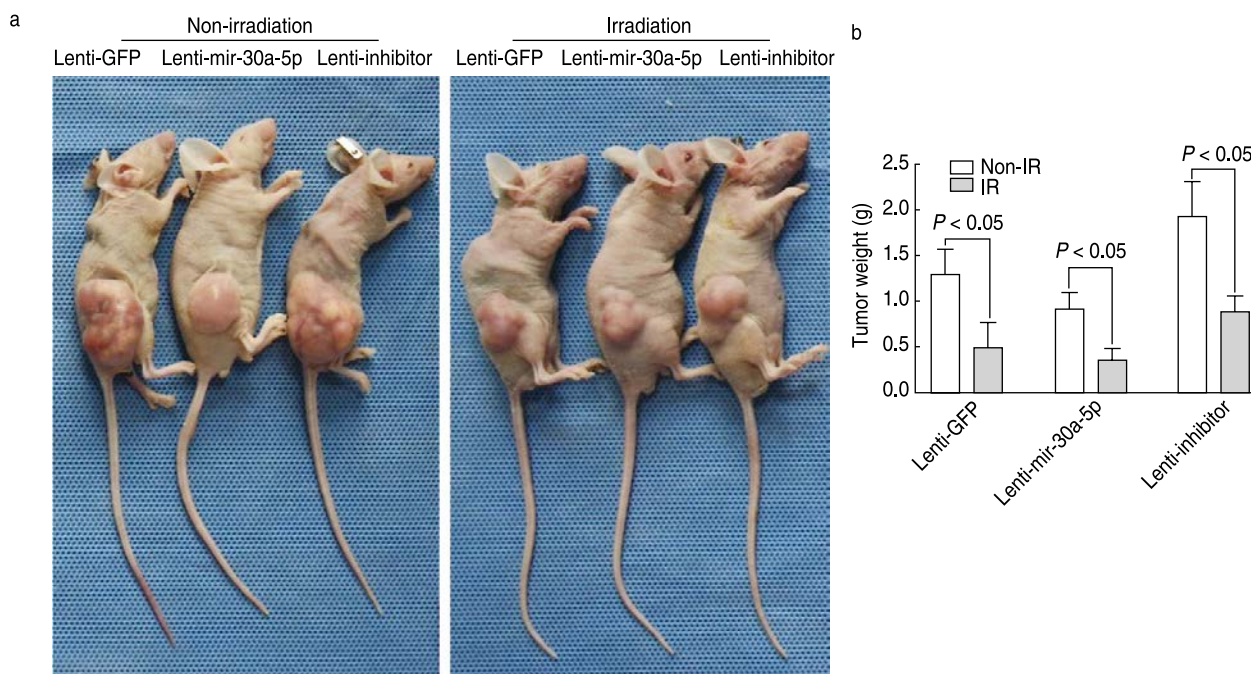


**Fig. 3** Tumor weight of nude mice in different treatment groups. (a) Representative picture of tumor-bearing nude mice; (b) Statistical chart tumor weight

30a-5p (lenti-mir-30a-5p + IR) groups were lower than those in the lenti-GFP groups. In contrast, both lenti-inhibitor groups showed higher tumor weights than those in the lenti-GFP groups (Fig. 3 and Table 3).

The tumor inhibition rate in the lenti-mir-30a-5p and lenti-mir-30a-5p + IR groups was 27.86 ± 7.02% and 18.75 ± 22.17%, respectively, compared to the corresponding lenti-GFP groups, indicating that overexpression of mir-30a-5p could increase the tumor inhibition rate of A549 cell line subcutaneous xenografts. Tumor inhibition rates were significantly higher in the all irradiated groups compared to the lenti-GFP group. However, inhibition rate was higher in the lenti-mir-30a-5p group (*P* > 0.05) than in the lenti-GFP + IR group, and lower in the lenti-inhibitor + IR group (*P* < 0.05) than in the lenti-GFP + IR

group (Table 3).

All nude mice lost weight when irradiation began compared to the not irradiated (*P* < 0.05; Fig. 4 and Table 3).

### Detecting the expression of radiosensitivity-related proteins by immunohistochemical method

H&E staining was used to confirm that tumor tissue had been obtained (Fig. 5). ATM protein expression level was lower in the lenti-mir-30a-5p group and higher in the lenti-inhibitor group than in the lenti-GFP group, with or without irradiation (*P* < 0.05; Fig. 6). The phosphorylation level of ATM at S1981 was low in the three groups without irradiation however, after

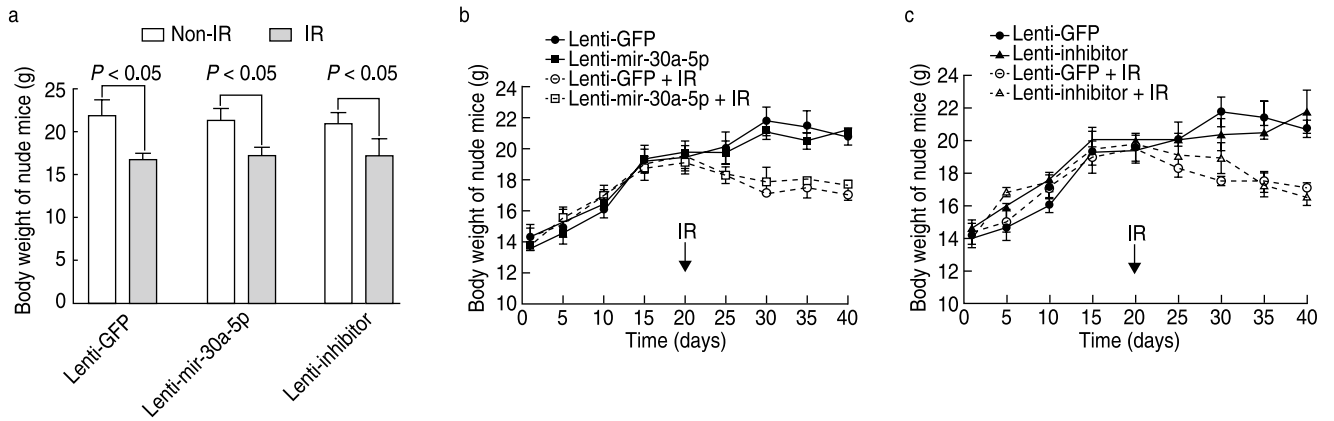


**Fig. 4** Body weight of nude mice in different treatment groups. (a) Body weight of nude mice; (b) Body weight changing curve: lenti-mir-30a-5p ± IR vs. lenti-GFP ± IR; (c) Body weight changing curve: lenti-inhibitor ± IR vs. lenti-GFP + IR

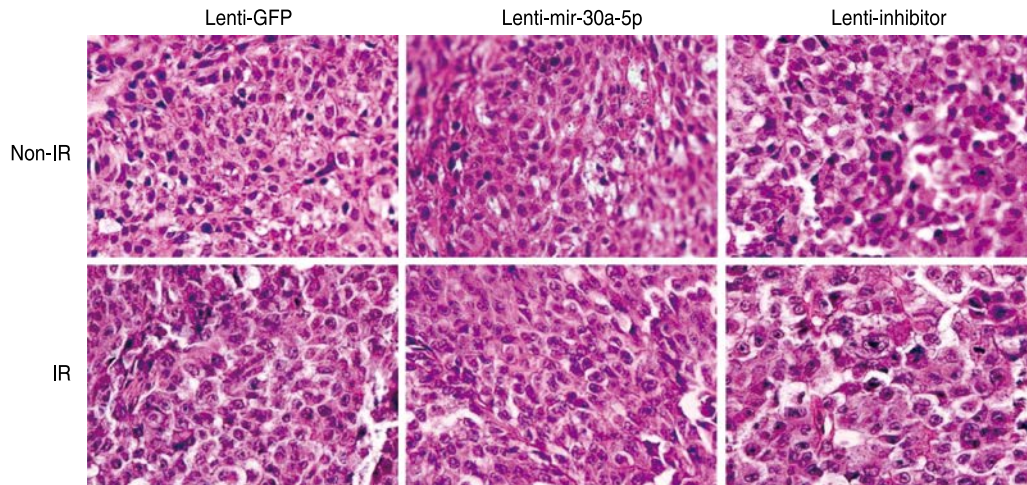


**Fig. 5** H&E staining in different groups (magnification ×400)

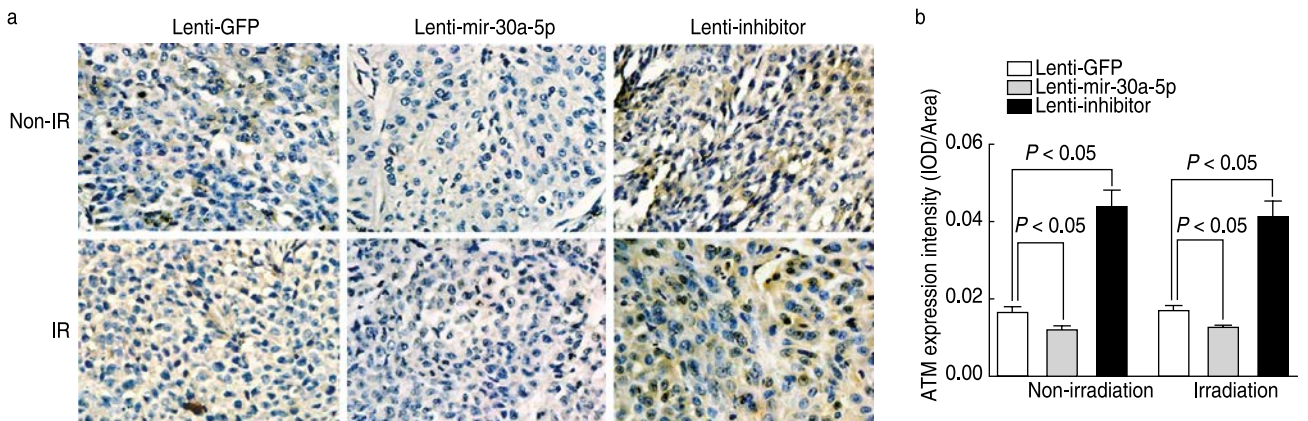


**Fig. 6** ATM protein expression in different treatment groups. (a) Immunohistochemical representative image of ATM protein expression (magnification ×400); (b) Statistical chart of ATM expression intensity

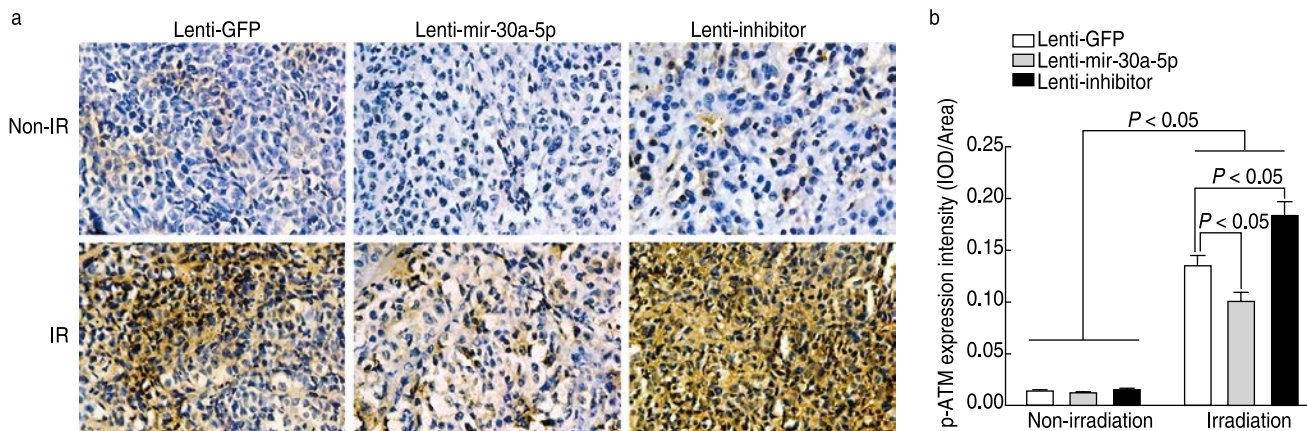


**Fig. 7** Phosphorylation level of ATM at S1981 in different treatment groups. (a) Immunohistochemical representative picture of ATM phosphorylation level (magnification  $\times 400$ ); (b) Statistical chart of p-ATM expression intensity

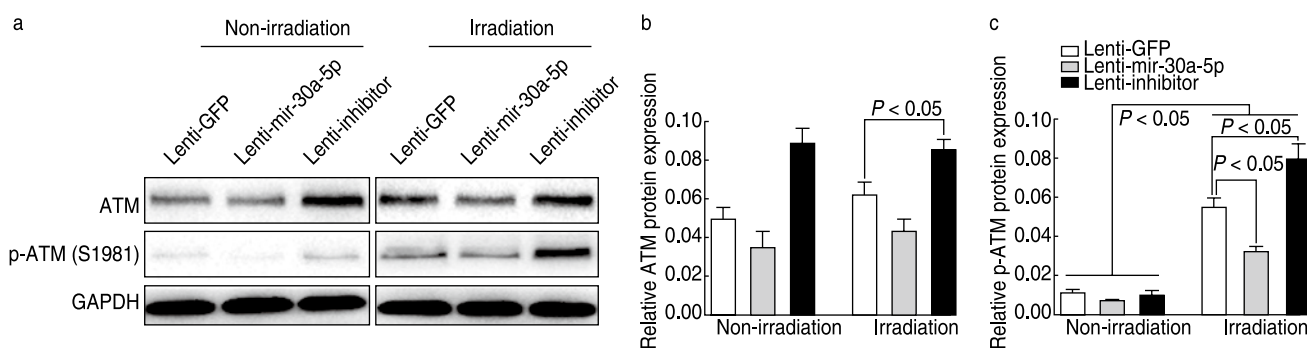


**Fig. 8** ATM protein expression and phosphorylation level of ATM at S1981 in different treatment groups. (a) Representative Western blot showing ATM protein expression and its phosphorylation level; (b) Statistical chart of relative ATM protein expression; (c) Statistical chart of relative p-ATM level

irradiation, it significantly increased in all treated groups ( $P < 0.05$ ). Moreover, it was higher in the lenti-mir-30a-5p + IR group and lower in the lenti-inhibitor + IR group than in the lenti-GFP + IR group ( $P < 0.05$ ; Fig. 7).

### Detecting the expression of radiosensitivity-related proteins by Western blotting

ATM protein expression level was lower in the lenti-mir-30a-5p group and higher in the lenti-inhibitor group than in the lenti-GFP group, with or without irradiation (Fig. 8a–8b). The phosphorylation level of ATM at S1981 was low in the three groups without irradiation however, it significantly increased ( $P < 0.05$ ) after irradiation. It was higher in the lenti-mir-30a-5p + IR group and lower in the lenti-inhibitor + IR group compared to the lenti-GFP + IR group ( $P < 0.05$ ; Fig. 8).

### Discussion

At present, a wide variety of miRNAs have been identified that may be related to cancer progression [19–21]. Many microRNAs are important radiosensitivity

regulators, which produce effects by interacting with the key factors involved in the regulation of radiosensitivity [2]. The expression level of mir-30a is diminished in many types of tumors, its expression is closely related to tumor progression and can play an inhibitory role in many types of tumors [22]. For example, gastric cancer [23], cholangiocarcinoma [15], esophageal cancer [24]. Further, mir-30a can affect tumor progression and therapeutic efficacy by regulating tumor cell proliferation [15], migration and invasion [16], EMT [25], apoptosis, and autophagy [17] (Fig. 9).

DNA is the primary target of radiation. The effect of radiation on tumors leads to the activation or inhibition of related genes, which could affect the radiosensitivity. ATM is an important effector of radiation-induced DNA damage [26]. ATM and ataxia telangiectasia and Rad3-related gene (ATR), as the core kinases in the whole process of DDR, can detect various forms of DNA damage and trigger downstream cascade reactions [11]. ATM, ATR, and DNA-PKcs are phosphatidylinositol-3 kinase-related kinase (PIKK) family members that play crucial roles in DNA damage repair [27]. ATR is activated by ultraviolet

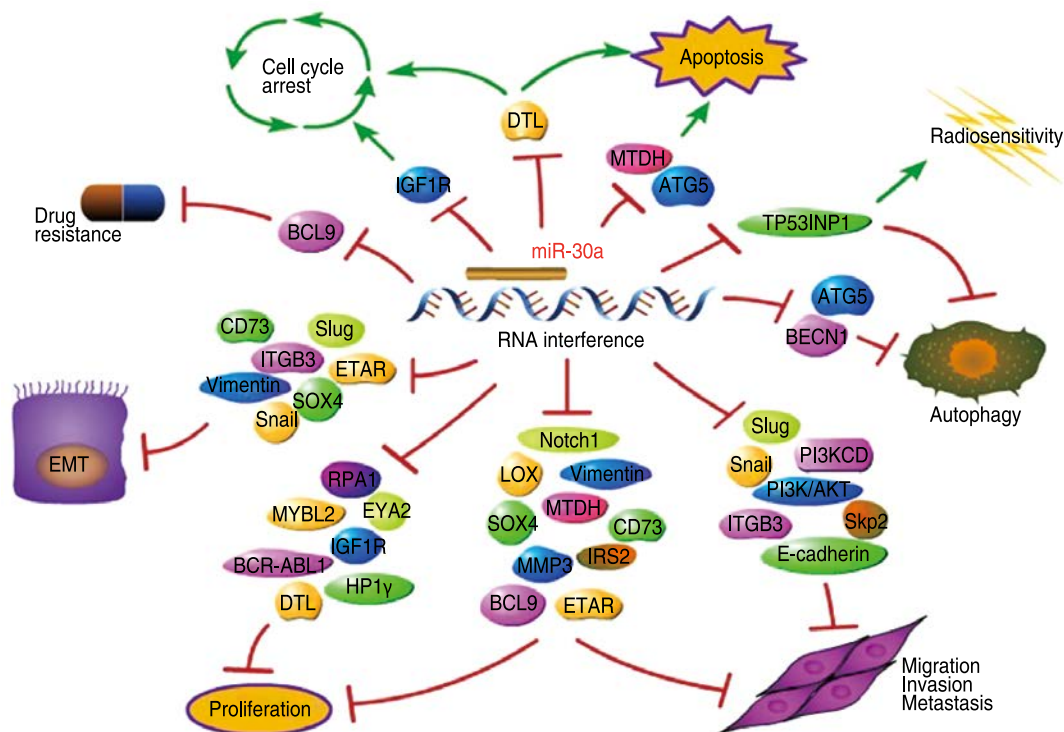


Fig. 9 Schematic diagram of the role of miR-30a in cancer

treatment or replication fork disintegration. ATM mainly affects radiation-induced DNA double-strand breaks and participates in cell reprogramming<sup>[28]</sup>. Mutations in ATM cause extreme sensitivity to radiation and increase tumor risk<sup>[14]</sup> and can also participate in the regulation of cell cycle checkpoints, DNA repair, and apoptosis<sup>[11]</sup>.

DNA damage can activate the phosphorylation of serine site 1981 of ATM, which activates a series of downstream effector molecules and participates in the regulation of the cell cycle, apoptosis, and DNA damage repair<sup>[29-30]</sup>, causing cells to be insensitive to radiation<sup>[11, 31]</sup>. Its downstream effectors include DNA-PK, Ku70/80, BRCA1, BRCA2, RAD51, and RAD52. These can participate in the regulation of various biological processes, such as non-homologous end-joining, homologous recombination, cell cycle checkpoints, and apoptosis regulation<sup>[12]</sup>. Poly ADP-ribose polymerase-1 is an important effect or molecule in the DDR pathway and participates in cell survival<sup>[32]</sup>. Inhibition of ATM and its downstream proteins could improve the radiosensitivity of tumors and hinder the DNA damage repair process<sup>[11, 33]</sup>.

In a previous study, we confirmed the low expression levels of miR-30a-5p in A549 and H460 cell lines *in vitro*, and its radiosensitizing effect on A549 cell lines<sup>[18]</sup>. Here, we confirmed this effect by using lentivirus to construct a subcutaneous xenograft model of lung cancer in nude mice and study it *in vivo*. The results showed

a slower tumor growth trend in the overexpression miR-30a-5p group after irradiation, compared to the control group. Smaller tumor volume, lower tumor weight and a higher tumor inhibition rate was observed compared to the control group. The miR-30a-5p downregulated group showed larger tumor volume, higher tumor weight and lower tumor inhibition rate than the control group. The results of immunohistochemistry and Western blotting suggested that the overexpression of miR-30a-5p could also inhibit the activation of ATM 1981 serine phosphorylation induced by radiation *in vivo*, thus improving the radiosensitivity of tumors. We plan to investigate the specific mechanism between miR-30a-5p and the ATM signaling pathway in future studies.

Some of the results in our study showed no statistical difference, which may be related to a late start time, early end time, or insufficient dose of radiation. The radiation dose and time may be the main factors affecting the experimental results. Due to limited experimental conditions, we performed whole-body irradiation of nude mice. In the radiation group, a series of systemic symptoms gradually appeared during the experiment, and the body weight of nude mice decreased significantly, which may have also interfered with the experimental results. However, there was no difference in the body weight of nude mice in the different miR-30a-5p expression groups, which also provided some theoretical support for the safety of miR-30a-5p *in vivo*.

## Conclusion

These results confirmed that mir-30a-5p has a radiosensitizing effect on the A549 cell lung cancer subcutaneous xenograft model in nude mice. Mir-30a-5p enhanced the radiosensitivity of nude mice with subcutaneous lung-cancer xenografts by inhibiting ATM phosphorylation.

In further studies, the radiation dose and time can be adjusted, the *in vivo* study can be detected more accurately, a lung transplant tumor model can be constructed, and further research can be performed in lung tissue, with the help of animal imaging and other techniques.

## Acknowledgments

Not applicable.

## Funding

This study was supported by the National Science Fund Project (No. 81872471) of the National Natural Science Foundation of China and the Science Foundation of the Second Affiliated Hospital of Xi'an Jiaotong University (No. YJ(QN)202025).

## Conflicts of interest

The authors indicated no potential conflicts of interest.

## Author contributions

All authors contributed to data acquisition and interpretation and reviewed and approved the final version of this manuscript.

## Data availability statement

Not applicable.

## Ethical approval

Animal experiments were performed in accordance with the ethical guidelines for experimental animals of the Department of Medicine, Xi'an Jiaotong University, China.

## References

- Cao H, Wang SL, Liu YH. Antitumor and vascular effects of apatinib combined with chemotherapy in mice with non-small-cell lung cancer. *Oncol Transl Med.* 2021;7(3):141-147.
- Zhao L, Bode AM, Cao Y, et al. Regulatory mechanisms and clinical perspectives of miRNA in tumor radiosensitivity. *Carcinogenesis.* 2012;33(11):2220-2227.
- Lindblom E, Dasu A, Toma-Dasu I. Optimal fractionation in radiotherapy for non-small cell lung cancer – a modelling approach. *Acta Oncol.* 2015;54(9):1592-1598.
- Berthel E, Ferlazzo ML, Devic C, et al. What does the history of research on the repair of DNA double-strand breaks tell us? – A comprehensive review of human radiosensitivity. *Int J Mol Sci.* 2019;20(21):5339.
- Zhang T, Shen Y, Chen Y, et al. The ATM inhibitor KU55933 sensitizes radioresistant bladder cancer cells with DAB2IP gene defect. *Int J Radiat Biol.* 2015;91(4):368-378.
- Tu W, Dong C, Konishi T, et al. G(2)-M phase-correlative bystander effects are co-mediated by DNA-PKcs and ATM after carbon ion irradiation. *Mutat Res Genet Toxicol Environ Mutagen.* 2016;795:1-6.
- Krause M, Dubrovskaja A, Linge A, et al. Cancer stem cells: Radioresistance, prediction of radiotherapy outcome and specific targets for combined treatments. *Adv Drug Deliv Rev.* 2017;109:63-73.
- Liang N, Zhong R, Hou X, et al. Ataxia-telangiectasia mutated (ATM) participates in the regulation of ionizing radiation-induced cell death via MAPK14 in lung cancer H1299 cells. *Cell Prolif.* 2015;48(5):561-572.
- Strom T, Harrison LB, Giuliano AR, et al. Tumour radiosensitivity is associated with immune activation in solid tumours. *Eur J Cancer.* 2017;84:304-314.
- Schaue D. A century of radiation therapy and adaptive immunity. *Front Immunol.* 2017;8:431.
- Estiar MA, Mehdipour P. ATM in breast and brain tumors: a comprehensive review. *Cancer Biol Med.* 2018;15(3):210-227.
- Zhao L, Lu X, Cao Y. MicroRNA and signal transduction pathways in tumor radiation response. *Cell Signal.* 2013;25(7):1625-1634.
- Toulany M, Mingjee M, Kehlbach R, et al. ErbB2 expression through heterodimerization with erbB1 is necessary for ionizing radiation- but not EGF-induced activation of Akt survival pathway. *Radiother Oncol.* 2010;97(2):338-345.
- Kerns SL, Ostrer H, Rosenstein BS. Radiogenomics: using genetics to identify cancer patients at risk for development of adverse effects following radiotherapy. *Cancer Discov.* 2014;4(2):155-165.
- Zhang JW, Wang X, Li GC, et al. MiR-30a-5p promotes cholangiocarcinoma cell proliferation through targeting SOCS3. *J Cancer.* 2020;11(12):3604-3614.
- Yu D, Liu H, Qin J, et al. Curcumin inhibits the viability and invasion of colorectal cancer cells via miR-30a-5p and Hippo signaling pathway. *Oncol Lett.* 2021;21(4):299.
- Chen W, Li Z, Liu H, et al. MicroRNA-30a targets BECLIN-1 to inactivate autophagy and sensitizes gastrointestinal stromal tumor cells to imatinib. *Cell Death Dis.* 2020;11(3):198.
- Guo Y, Sun W, Gong T, et al. miR-30a radiosensitizes non-small cell lung cancer by targeting ATF1 that is involved in the phosphorylation of ATM. *Oncol Rep.* 2017;37(4):1980-1988.
- Fan T, Wang CQ, Zhang K, et al. Differentially expressed genes analysis and target genes prediction of miR-22 in breast cancer. *Oncol Transl Med.* 2021;7(2):59-64.
- Zhang CL, Liu D, Tian QQ, et al. CircBAGE2 (hsa\_circ\_0061259) regulates CCND1 and PDCD10 expression by functioning as a miR-103a-3p 'sponge' to alter the proliferation and apoptosis of prostate cancer cells. *Oncol Transl Med.* 2021;7(5):221-228.
- Hao TT, Wang CQ, Song YJ, et al. Relationship between miR-7-5p expression and <sup>125</sup>I seed implantation efficacy in pancreatic cancer and functional analysis of target genes. *Oncol Transl Med.* 2021;7(4):177-182.
- Zhao JJ, Lin J, Zhu D, et al. miR-30-5p functions as a tumor suppressor and novel therapeutic tool by targeting the oncogenic Wnt/β-catenin/BCL9 pathway. *Cancer Res.* 2014;74(6):1801-1813.
- Min J, Han TS, Sohn Y, et al. microRNA-30a arbitrates intestinal-type early gastric carcinogenesis by directly targeting ITGA2. *Gastric Cancer.* 2020;23(4):600-613.

24. Butz F, Eichelmann AK, Mayne GC, et al. MicroRNA profiling in oesophageal adenocarcinoma cell lines and patient serum samples reveals a role for miR-451a in radiation resistance. *Int J Mol Sci.* 2020;21(23):8898.
25. Zhang Y, Li Y. Long non-coding RNA NORAD contributes to the proliferation, invasion and EMT progression of prostate cancer via the miR-30a-5p/RAB11A/WNT/ $\beta$ -catenin pathway. *Cancer Cell Int.* 2020;20(1):571.
26. Pizzamiglio L, Focchi E, Antonucci F. ATM protein kinase: Old and new implications in neuronal pathways and brain circuitry. *Cells.* 2020;9(9):1969.
27. Balmus G, Pilger D, Coates J, et al. ATM orchestrates the DNA-damage response to counter toxic non-homologous end-joining at broken replication forks. *Nat Commun.* 2019;10(1):87.
28. Kinoshita T, Nagamatsu G, Kosaka T, et al. Ataxia-telangiectasia mutated (ATM) deficiency decreases reprogramming efficiency and leads to genomic instability in iPS cells. *Biochem Biophys Res Commun.* 2011;407(2):321-326.
29. Neumann J, Yang Y, Köhler R, et al. Mangrove dolabrane-type of diterpenes tagalsins suppresses tumor growth via ROS-mediated apoptosis and ATM/ATR-Chk1/Chk2-regulated cell cycle arrest. *Int J Cancer.* 2015;137(11):2739-2748.
30. Khoronenkova SV, Dianov GL. ATM prevents DSB formation by coordinating SSB repair and cell cycle progression. *Proc Natl Acad Sci USA.* 2015;112(13):3997-4002.
31. Rondeau S, Vacher S, De Koning L, et al. ATM has a major role in the double-strand break repair pathway dysregulation in sporadic breast carcinomas and is an independent prognostic marker at both mRNA and protein levels. *Br J Cancer.* 2015;112(6):1059-1066.
32. Menolfi D, Zha S. ATM, ATR and DNA-PKcs kinases – the lessons from the mouse models: inhibition  $\neq$  deletion. *Cell Biosci.* 2020;10:8.
33. Langelier MF, Pascal JM. PARP-1 mechanism for coupling DNA damage detection to poly(ADP-ribose) synthesis. *Curr Opin Struct Biol.* 2013;23(1):134-143.

**DOI 10.1007/s10330-021-0534-4**

**Cite this article as:** Guo YY, Cui YT, Bao X, et al. Radiosensitization by microRNA30a-5p in a nude mouse model with subcutaneous lung-cancer xenograft. *Oncol Transl Med.* 2022;8(4):155-164.